



UNIVERSITY OF LEEDS

This is a repository copy of *On the secular trend of CO<sub>x</sub> and CO<sub>2</sub> in the lower thermosphere.*

White Rose Research Online URL for this paper:  
<http://eprints.whiterose.ac.uk/131572/>

Version: Accepted Version

---

**Article:**

Garcia, RR, López-Puertas, M, Funke, B et al. (3 more authors) (2016) On the secular trend of CO<sub>x</sub> and CO<sub>2</sub> in the lower thermosphere. *Journal of Geophysical Research: Atmospheres*, 121 (7). pp. 3634-3644. ISSN 2169-897X

<https://doi.org/10.1002/2015JD024553>

---

©2016. American Geophysical Union. This is an author produced version of a paper published in *Journal of Geophysical Research: Atmospheres*. Uploaded in accordance with the publisher's self-archiving policy.

**Reuse**

Items deposited in White Rose Research Online are protected by copyright, with all rights reserved unless indicated otherwise. They may be downloaded and/or printed for private study, or other acts as permitted by national copyright laws. The publisher or other rights holders may allow further reproduction and re-use of the full text version. This is indicated by the licence information on the White Rose Research Online record for the item.

**Takedown**

If you consider content in White Rose Research Online to be in breach of UK law, please notify us by emailing [eprints@whiterose.ac.uk](mailto:eprints@whiterose.ac.uk) including the URL of the record and the reason for the withdrawal request.



[eprints@whiterose.ac.uk](mailto:eprints@whiterose.ac.uk)  
<https://eprints.whiterose.ac.uk/>

1

2

3

**On the secular trend of CO<sub>x</sub> and CO<sub>2</sub> in the lower thermosphere**

4

5

Rolando R. Garcia<sup>1</sup>, Manuel López-Puertas<sup>2</sup>, Bernd Funke<sup>2</sup>, Douglas E. Kinnison<sup>1</sup>,

6

Daniel R. Marsh<sup>1</sup>, and Liying Qian<sup>1</sup>

7

8

9

10

11

12

13

14 <sup>1</sup>National Center for Atmospheric Research, Boulder, CO, USA

15 <sup>2</sup>Instituto de Astrofísica de Andalucía, CSIC, Granada, Spain

16 Corresponding author: R. R. Garcia, National Center for Atmospheric Research, Boulder,

17 CO, 80307-3000, USA (rgarcia@ucar.edu)

18

19 **Key points:**

- 20 • Observations suggest that CO<sub>2</sub> in the lower thermosphere has increased rapidly  
21 since the early 2000s.
- 22 • The observed behavior cannot be simulated by a comprehensive climate-chemistry  
23 model.
- 24 • Model and observations could be reconciled if vertical eddy mixing has increased  
25 by about 30% per decade.

## Abstract

26  
27  
28 An analysis of recent observations (2004-2013) made by the ACE-FTS instrument  
29 indicate that total carbon ( $\text{CO}_x = \text{CO} + \text{CO}_2$ ) has been increasing rapidly in the lower  
30 thermosphere, above  $10^{-3}$  hPa (90 km). The estimated trend ( $\sim 9\%$  per decade) is about a  
31 factor of two larger than the rate of increase that can be ascribed to anthropogenic  
32 emissions of  $\text{CO}_2$  ( $\sim 5\%$  per decade). Here we investigate whether the observed trends of  
33  $\text{CO}_2$  and  $\text{CO}_x$  can be reproduced using the Whole Atmosphere Community Climate Model  
34 (WACCM), a comprehensive global model with interactive chemistry, wherein vertical  
35 eddy diffusion is estimated from a parameterization of gravity wave breaking that can  
36 respond to changes in the model climate. We find that the modeled trends of  $\text{CO}_2$  and  $\text{CO}_x$   
37 do not differ significantly at any altitude from the value expected from anthropogenic  
38 increases of  $\text{CO}_2$ , and that WACCM does not produce significant changes in eddy  
39 diffusivity. We show that the discrepancy between model and observations cannot be  
40 attributed to uncertainties associated with geophysical noise and instrumental effects, to  
41 difficulties separating a linear trend from the 11-year solar signal, or to sparse sampling by  
42 ACE-FTS. Estimates of the impact of vertical diffusion on  $\text{CO}_2$  in the model indicate that a  
43 large increase in  $K_{zz}$  ( $\sim 30\%$  per decade) would be necessary to reconcile WACCM results  
44 with observations. It might be possible to ascertain whether such a large change in vertical  
45 mixing has in fact taken place by examining the trend of water vapor in the upper  
46 mesosphere.

47 **1. Introduction.**

48 *Emmert et al.* (2012) calculated the global linear trend of CO<sub>x</sub> (the sum of CO and  
49 CO<sub>2</sub>) from observations made by the Atmospheric Chemistry Experiment Fourier  
50 Transform Spectrometer (ACE-FTS) between April 2004 and September 2011, and  
51 documented a very fast rate of increase at altitudes above about 10<sup>-3</sup> hPa (~90 km). Near  
52 100 km, the linear trend of CO<sub>x</sub> was approximately 9% per decade, which is much faster  
53 than the anthropogenic rate of increase of CO<sub>2</sub> in the lower atmosphere for the period in  
54 question (~5% per decade). *Emmert et al.* analyzed the trend in CO<sub>x</sub> in order to minimize  
55 the effects of the solar cycle on CO<sub>2</sub>, since the photolysis of this gas by UV radiation  
56 (which produces CO) becomes important above 90 km and varies strongly with solar  
57 activity. Insofar as CO<sub>2</sub> represents the bulk of CO<sub>x</sub> below about 100 km, *Emmert et al.*  
58 ascribed the trend in CO<sub>x</sub> to increases in CO<sub>2</sub>. They also showed, using a one-dimensional  
59 model with interactive chemistry [*Roble*, 1995], that the observed trend in CO<sub>x</sub> could be  
60 due to a corresponding trend in vertical eddy diffusion of 15% per decade, since such a  
61 trend would increase the rate of transport of CO<sub>2</sub> into the lower thermosphere. Indeed,  
62 *Garcia et al.* [2014] have shown that, in the range of altitude 90-105 km (about 10<sup>-3</sup> to 10<sup>-4</sup>  
63 hPa), the mixing ratio of CO<sub>2</sub> is controlled principally by the competition between eddy  
64 diffusion and molecular diffusive separation.

65 *Emmert et al.*'s conclusions regarding a fast rate of increase of CO<sub>2</sub> in the lower  
66 thermosphere are supported by the recent study of *Yue et al.* [2015], who used SABER  
67 (Sounding of the Atmosphere by Broadband Emission Radiometry) observations from 2002  
68 through 2014, and estimated a rate of increase of CO<sub>2</sub> exceeding 10% per decade above  
69 100 km. While SABER observations do not include CO, *Yue et al.* performed a multiple

70 linear regression that included the solar 10.7 cm radio flux as a predictor to account for the  
71 influence of solar activity on CO<sub>2</sub>.

72 Here we investigate whether the large trends of CO<sub>2</sub> and CO<sub>x</sub> in the upper atmosphere  
73 derived from observations can be reproduced in simulations made with the Whole  
74 Atmosphere Community Climate Model (WACCM), a three-dimensional, global climate  
75 model with interactive chemistry. The model is discussed briefly in Section 2, with  
76 emphasis on the question of transport in the mesosphere and lower thermosphere (MLT),  
77 which is dominated by the divergence of vertical eddy fluxes due to breaking gravity  
78 waves. While these small-scale waves cannot be simulated explicitly at the relatively coarse  
79 spatial and temporal resolutions used in a climate model, they are parameterized in such a  
80 way that they can respond to changes in the model's climate.

81 In Section 3, we compare updated ACE-FTS observations that span the period 2004  
82 through 2013 with WACCM simulations of the same period to show that the simulated CO  
83 and CO<sub>2</sub> agree well with the observations in the lower thermosphere. In Section 4, we  
84 derive trends in CO<sub>x</sub> and CO<sub>2</sub> from the ACE-FTS data and compare them with trends  
85 derived from WACCM output, and with the earlier estimates of *Emmert et al.* [2012]. The  
86 trends derived from the data are consistent with the findings of *Emmert et al.*, and are much  
87 larger than the model trends above 90 km. In fact, WACCM-derived trends in the lower  
88 thermosphere are not significantly different from the trends below the mesopause, which  
89 are ascribable to anthropogenic emissions of CO<sub>2</sub>. We go on to examine several possible  
90 sources of uncertainty that might account for the discrepancy between observed and  
91 modeled trends, and conclude that none can explain the differences between the model and  
92 the observations. Finally, we estimate the impact of increases in vertical eddy diffusion on

93 the trends computed with WACCM, and find that a rather large  $K_{zz}$  trend, of over 30% per  
94 decade, would be needed to reconcile the model with the observations. In Section 5, we  
95 summarize our findings and suggest additional observations that might be useful for  
96 ascertaining whether such increases in vertical eddy diffusion might have taken place in the  
97 Earth’s upper atmosphere.

## 98 **2. Numerical model**

99 The Whole Atmosphere Community Climate Model (WACCM) is a global climate  
100 model with interactive chemistry that spans the range of altitude 0-140 km. In this study,  
101 we use the “specified dynamics” version (SD-WACCM), described by *Garcia et al.* [2014].  
102 In SD-WACCM, winds and temperature are constrained by NASA’s Modern-Era  
103 Retrospective Analysis (MERRA) data [*Rienecker et al.*, 2011] everywhere below  
104 approximately 1 hPa, using the procedure discussed by *Kunz et al.* [2011]. The use of SD-  
105 WACCM for the present investigation is motivated by the desire to study the particular  
106 period, 2004 through 2013, covered by the ACE-FTS observations described in the next  
107 section. While SD-WACCM is free running above 1 hPa, *Liu et al.* [2009] have shown that  
108 the dynamics of the mesosphere and lower thermosphere are strongly influenced by the  
109 behavior of the lower atmosphere. In the remainder of this paper, we refer to the model  
110 simply as WACCM, with the understanding that all simulations have been carried out with  
111 the specified dynamics version.

112 The reader is referred to the study of *Garcia et al.* [2014] for additional details of the  
113 specified dynamics configuration. Here, we emphasize only the parameterization of small-  
114 scale gravity waves, since vertical mixing due to gravity wave breaking is the principal

115 upward transport mechanism in the lower thermosphere, below  $10^{-4}$  hPa, particularly in the  
116 global-mean sense. The gravity wave parameterization attempts to take into account the  
117 excitation of mesoscale waves by various physical mechanisms, such as flow over  
118 orography, deep convection, and frontal zones. Non-orographic gravity wave source  
119 spectra are dependent on convective heat release in the Tropics and frontal zones diagnosed  
120 in extra-tropical latitudes, as described in detail by *Richter et al.* [2010]. Because  
121 parameterized gravity wave sources are related to physical processes simulated in the  
122 underlying global model, their behavior can potentially change as the model climate  
123 changes. For example, the source spectra will change if the characteristics of convection or  
124 the frequency or intensity of fronts diagnosed in the model changes; and the propagation of  
125 the waves to the MLT will be influenced by the behavior of the zonal-mean zonal wind  
126 systems in the stratosphere.

127 We note that the effective value of  $K_{zz}$  calculated with WACCM depends also on the  
128 value assumed for the Prandtl number,  $Pr$ , which describes the ratio of the eddy momentum  
129 flux to the eddy flux of potential temperature or chemical species [see *Garcia et al.*, 2007].  
130 The value used in the study of *Garcia et al.* [2014] was  $Pr = 4$ . As discussed in that study,  
131 comparison of simulated and observed CO and CO<sub>2</sub> suggests that a smaller value,  $Pr = 2$ ,  
132 might be more appropriate; therefore, we use simulations made with  $Pr = 2$  to compute  
133 model trends in this study. Nevertheless, in Section 4 we use results from our earlier  
134 simulation with  $Pr = 4$  to estimate the potential impact of changes in  $K_{zz}$  on the trends of  
135 CO<sub>x</sub> and CO<sub>2</sub>. (It should be notedemphasized, however, that the trends of CO<sub>2</sub> and CO<sub>x</sub> in  
136 WACCM are insensitive to  $Pr$  as long as the value of  $Pr$  is constant throughout the  
137 simulation).

138 **3. Comparison of observed and modeled CO and CO<sub>2</sub>**

139 The Atmospheric Chemistry Experiment Fourier Transform Spectrometer (ACE-FTS)  
140 on SCISAT-1 has been making solar occultation measurements of CO and CO<sub>2</sub> since 2004  
141 [Boone *et al.*, 2005; Clerbaux *et al.*, 2008; Beagley *et al.*, 2010]. CO<sub>2</sub> volume mixing ratio  
142 (vmr) is retrieved from 50 to 120 km; the vertical resolution averages 3-4 km, varying from  
143 2 to 6 km depending on the time of the year. Random errors are 2.5-5%, depending on  
144 latitude, and systematic errors range from 2% at the low altitudes (50-70 km) to about 5%  
145 at 90 km, 9% at 100 km, and 16% at 118.5 km [Beagley *et al.*, 2010]. CO vmr is retrieved  
146 in the range from 8 km to about 100 km [Clerbaux *et al.*, 2008]. The vertical resolution  
147 above about 1 hPa is about 4 km, degrading to 6 km in the upper mesosphere. The random  
148 errors of the CO measurements are < 10% in the mesosphere and lower thermosphere;  
149 systematic errors are < 25% from 30 to 100 km. The ACE-FTS observations, as well as the  
150 data screening procedures employed, are discussed in more detailed by Garcia *et al.*  
151 [2014]. The data used here is version 3.5 [Boone *et al.*, 2013] and was obtained from the  
152 ACE Science Team at the University of Waterloo, Canada. We note that ACE observations  
153 are processed in geometric coordinates. However, the final data products are provided in  
154 both geometric and pressure coordinates, and we use data in pressure coordinates in all  
155 comparisons with WACCM.

156 CO has also been observed by the Michelson Interferometer for Passive Atmospheric  
157 Sounding (MIPAS) using the “middle atmosphere” and “upper atmosphere” modes  
158 [Oelhaf, 2008], which cover the altitude ranges 20-102 km and 40-170 km, respectively.  
159 The vertical resolution of the MIPAS CO profiles is 4–7 km below 60 km at night and  
160 below 95 km during daytime, and 7-14 km above those altitudes. The single-measurement

161 precision (noise error) is 40-80% below 60 km, and 30-60% above, while the systematic  
162 error is estimated to range between 8 and 15 % [Funke *et al.*, 2009]. The MIPAS data are  
163 also discussed in detail by Garcia *et al.* [2014].

164 Figure 1 shows time series of WACCM CO and CO<sub>2</sub> together with observations at  
165 several levels in the lower thermosphere:  $6 \times 10^{-5}$  hPa (~108 km),  $2 \times 10^{-4}$  hPa (~100 km)  
166 and  $10^{-3}$  hPa (~90 km). For CO<sub>2</sub>, WACCM is within 10% of the ACE-FTS observations at  
167 all levels except  $6 \times 10^{-5}$  hPa, where the differences reach 15-20%. While the discrepancies  
168 are not large compared to the measurement errors for ACE-FTS, WACCM results for CO<sub>2</sub>  
169 are uniformly low in all cases. For CO, the WACCM simulation is generally closer to  
170 observations, especially given the large measurement errors. However, at  $10^{-3}$  hPa,  
171 WACCM CO is systematically higher than both ACE-FTS and MIPAS. In spite of these  
172 discrepancies, WACCM reproduces well the long-term variability of the data, which is  
173 dominated by the solar cycle, in particular at the higher altitudes.

174 The effect of the solar cycle can be largely removed by considering total carbon, CO<sub>x</sub>,  
175 which in the lower thermosphere is essentially the sum of CO and CO<sub>2</sub>. Figure 2 shows a  
176 comparison of modeled and observed CO<sub>x</sub> at  $10^{-3}$  and  $2 \times 10^{-4}$  hPa, two levels where both  
177 CO and CO<sub>2</sub> are measured by ACE-FTS. Since CO<sub>x</sub> at these levels is dominated by CO<sub>2</sub>,  
178 the agreement is within 10%, as was the case for CO<sub>2</sub> in Figure 1, with WACCM being  
179 systematically low compared to ACE-FTS. In both model and observations, the evolution  
180 of CO<sub>x</sub> shows mainly an increasing trend, with no indication of any solar cycle influence.  
181 The rate of increase of CO<sub>x</sub> is clearly faster in ACE-FTS than in WACCM, and this  
182 difference will be quantified in the next section, where we calculate linear trends. An  
183 additional difference between model and observations, both for CO<sub>x</sub> and for CO and CO<sub>2</sub>

184 individually, is that the observations exhibit considerably larger short-term variability than  
185 the model. The potential effect of this difference on the calculation of trends from  
186 WACCM output will be addressed below.

#### 187 4. Calculation and comparison of linear trends

188 Time series of CO<sub>x</sub> in WACCM are constructed from monthly-mean, globally  
189 averaged output for CO and CO<sub>2</sub>. The model output was de-seasonalized by subtracting the  
190 composite monthly seasonal cycle for the period 2004-2013 at each model level. ACE-FTS  
191 data were treated here in the same way as the WACCM output; that is, de-seasonalized,  
192 global monthly averages were calculated from the data on each pressure level. This differs  
193 from the procedure employed by *Emmert et al.* [2012] but yields very similar trends, as  
194 shown below.

195 We characterize the long-term behavior of CO<sub>x</sub> in the 10-year period 2004 to 2013 in  
196 terms of the linear trend obtained from a multiple linear regression (MLR). The regression  
197 model used is:

$$198 \quad \psi = a + b \cdot t + c \cdot s(t) + d \cdot qbo_1(t) + e \cdot qbo_2(t) \quad (1)$$

199 where  $t$  is time;  $s$  is a solar cycle predictor, here taken to be the 10.7 cm radio flux; and  
200  $qbo_1$ , and  $qbo_2$  are two linearly independent indices of the quasi-biennial oscillation (QBO),  
201 represented by the zonal-mean zonal wind at 10 and 30 hPa, respectively. The  
202 autocorrelation of the residuals of the fit was taken into account when estimating the  
203 uncertainty of the trend [*Tiao et al.*, 1990]. No attempt was made to include in the MLR  
204 predictors for ENSO (El Niño-Southern Oscillation) or for volcanic eruptions. In practice, it  
205 turns out that even the QBO predictors explain a negligible fraction of the variance of CO<sub>x</sub>

206 in the lower thermosphere. Likewise, the solar predictor turns out to be relatively  
207 unimportant at the altitudes (below about 105 km) where CO<sub>x</sub> data are available from ACE-  
208 FTS. Note that this is not true of CO<sub>2</sub> alone, which is photolyzed by UV radiation to  
209 produce CO. However, the combination of CO and CO<sub>2</sub> into a total carbon variable, CO<sub>x</sub>,  
210 has the desirable effect of minimizing the impact of the solar cycle on the MLR.

211 Figure 3 compares the vertical profile of the linear trend coefficient, *b*, obtained when  
212 the MLR defined by Eq. (1) is applied to ACE-FTS observations and to WACCM output.  
213 Three things are immediately obvious from the figure: The trend calculated from ACE-FTS  
214 measurements reaches a maximum of 8.5% at 95-100 km, consistent with the results of  
215 *Emmert et al.* [2002], who analyzed a shorter period (2004-2011); the trend calculated from  
216 WACCM output in the lower thermosphere is statistically indistinguishable from the trend  
217 at lower altitudes; and the WACCM trend is significantly different from that derived from  
218 ACE-FTS observations in the lower thermosphere, between  $2 \times 10^{-3}$  hPa (~85 km) and  $2 \times$   
219  $10^{-4}$  hPa (~100 km). As in *Emmert et al.*, our estimate of the ACE-FTS trend below 80 km  
220 (~ $10^{-2}$  hPa) is influenced by *a priori* assumptions about CO<sub>2</sub> inherent in the ACE-FTS  
221 retrieval, which yield too low a trend for the period under examination. However, as noted  
222 by *Emmert et al.*, this does not affect the estimate of the trend above 90 km (~ $10^{-3}$  hPa).

223 We consider next whether the statistical significance of the WACCM-ACE differences  
224 might be exaggerated because WACCM CO<sub>x</sub> has substantially less short-term variability  
225 than ACE-FTS data. Specifically, the WACCM time series shown in Figures 1 and 2 are  
226 constructed from true zonal means averaged globally over latitude, whereas ACE-FTS solar  
227 occultation observations are much more sparse, both in longitude and latitude, and in time,  
228 and they are subject to measurement errors not present in WACCM. A cursory

229 examination of Figures 1 and 2 reveals that the high-frequency variability is about a factor  
230 of 2 larger in the ACE-FTS time series than in the WACCM time series. We therefore test  
231 the sensitivity of the WACCM trends to the addition of “random noise”, which we  
232 simulate simply by adding to the time series of WACCM CO and CO<sub>2</sub> a series of normally  
233 distributed pseudo-random numbers, multiplied times the standard deviation of the original  
234 time series at each altitude; this has the effect of increasing the standard deviation of the  
235 resulting “noisy” time series by about a factor of  $\sqrt{2}$  compared to the original. As a result,  
236 the high-frequency variability of the treated WACCM output is similar to that seen in ACE-  
237 FTS data (not shown). The linear CO<sub>x</sub> trend profile extracted from the WACCM output  
238 with added noise is shown in Figure 4. While the uncertainty of the trend is much larger  
239 than for the original WACCM output (Figure 3) the trend in the thermosphere remains  
240 statistically undistinguishable from the trend at lower altitudes, and statistically different  
241 from the ACE-FTS trend between about 85 and 100 km.

242 We have also tested whether uncertainties in our knowledge of 11-year solar variability  
243 at UV wavelengths might influence the CO<sub>x</sub> trend derived from WACCM. As discussed by  
244 *Ermolli et al.* [2013], recent measurements of spectral solar irradiance (SSI) variability  
245 differ substantially from estimates based on empirical models. In particular, *Ball et al.*  
246 [2014] show that the 11-year variability observed by the SOLSTICE instrument onboard  
247 NASA’s SORCE satellite is much larger at wavelengths < 300 nm than predicted by  
248 models such as NRLSSI [*Lean et al.*, 1997] and SATIRE [*Krivova et al.*, 2011]. For CO<sub>x</sub>,  
249 we are interested in the range of wavelength 121-200 nm, which dominates CO<sub>2</sub> photolysis  
250 below ~105 km [cf. *Garcia et al.*, 2014; their Figure 1]. At these wavelengths, SSI changes  
251 over the 11-year solar cycle are about a factor of two larger in SOLSTICE observations

252 than in either of the aforementioned models. SSI in WACCM is prescribed using the  
253 NRLSSI model, so we adjusted SSI variability in the range 120-200 nm to be twice as  
254 predicted by this model, with no changes elsewhere in the spectrum, and carried out a new  
255 simulation of the period 2004-2013. The resulting CO<sub>x</sub> trend profile is compared with the  
256 original trend profile in Figure 5. It is evident that the larger SSI variability at 120-200 nm  
257 introduces little additional uncertainty in the WACCM CO<sub>x</sub> trend, even at 100 km. This is  
258 not wholly surprising because the use of CO<sub>x</sub> is intended to minimize the effect of solar  
259 variability on the estimate of the long-term trend. In addition, as shown by *Garcia et al.*  
260 [2014] (cf. their Figure 9), the mixing ratio of CO<sub>2</sub> below 10<sup>-4</sup> hPa (~105 km) is determined  
261 mainly by the competition between vertical eddy diffusion due to gravity wave breaking  
262 and molecular diffusive separation, with a smaller influence from UV photolysis.

263 Finally, we have considered whether the sparse sampling inherent in solar occultation  
264 observations might contribute to the differences in the trend profiles derived from ACE-  
265 FTS and WACCM. To investigate this possibility, we extracted WACCM vertical profiles  
266 of CO and CO<sub>2</sub> at the geo-locations (longitude, latitude, and time) nearest to ACE-FTS  
267 observations for the period 2004-2013. We then performed a trend analysis after processing  
268 the data as described by *Emmert et al.* [2012], with one exception: we regressed the  
269 WACCM output on both time (the linear trend) and on the solar f10.7 cm radio flux. As  
270 noted previously, regression on a solar predictor does not affect the results below 10<sup>-4</sup> hPa  
271 (~105 km), although it becomes increasingly important at higher altitudes, where CO<sub>x</sub> is no  
272 longer conserved due to differences in molecular diffusion between CO and CO<sub>2</sub>. The  
273 resulting trend profile is shown in Figure 6. It is clear that, even when the model is sampled

274 using the ACE geo-locations, the WACCM trend is significantly smaller than the ACE-FTS  
275 trend at altitudes between about 85 and 100 km.

## 276 **5. Summary and Discussion**

277 The results presented above show that the global trend of  $\text{CO}_x$  in the lower  
278 thermosphere calculated with WACCM is not significantly different from the trend  
279 ascribable to anthropogenic increases in  $\text{CO}_2$ , and that this trend (nowhere larger than  
280 5.5%) is much smaller than the trend calculated from ACE-FTS observations (8-9% per  
281 decade in the lower thermosphere). We have also shown that, even when we consider  
282 several plausible sources of uncertainty that might affect the WACCM  $\text{CO}_x$  trend, that trend  
283 remains smaller and statistically different from the ACE-FTS trend in the lower  
284 thermosphere.

285 *Emmert et al.* [2012] suggested that the  $\text{CO}_x$  trend derived from ACE-FTS  
286 observations could be explained if the rate of eddy diffusive transport of  $\text{CO}_2$  into the lower  
287 thermosphere was itself increasing. We have examined the evolution of the vertical  
288 diffusion coefficient,  $K_{zz}$ , estimated from the gravity wave parameterization in WACCM  
289 and find no statistical significant trend anywhere in the model domain during the period  
290 under consideration, 2004-2013; this is consistent with the lack of any trend in  $\text{CO}_2$  or  $\text{CO}_x$   
291 in the model beyond that due to anthropogenic emissions.

292 The value of  $K_{zz}$  in WACCM is predicted by the gravity wave parameterization  
293 interactively with the underlying, resolved dynamics, and cannot easily be adjusted *ad hoc*.  
294 However, we can estimate the impact of  $K_{zz}$  on chemical species by comparing otherwise  
295 identical simulations made with a different value of the Prandtl number,  $Pr$ , which

296 describes the ratio of the eddy momentum flux to the eddy flux of chemical species [see  
297 *Garcia et al.*, 2007]. In particular, halving  $Pr$  has the effect of increasing the effective  
298 magnitude of  $K_{zz}$  by approximately a factor of two. As noted in Section 2, the simulations  
299 examined thus far were made using  $Pr = 2$ , but we also have at hand earlier simulations,  
300 discussed by *Garcia et al.* [2014], that used  $Pr = 4$ . By comparing CO and CO<sub>2</sub> across the  
301 simulations, we can ascertain the impact of doubling  $K_{zz}$  on these species. Then, if we  
302 assume that changes in CO and CO<sub>2</sub> are linear in  $K_{zz}$ , we can estimate the impact of smaller  
303 changes in  $K_{zz}$  acting over one decade, and thus estimate the decadal trend in eddy diffusion  
304 that is necessary to bring WACCM CO<sub>x</sub> trends into agreement with ACE-FTS trends.

305 Figure 7 shows the estimated effect on the WACCM CO<sub>x</sub> trend of increasing  $K_{zz}$  at  
306 various rates. The figure reproduces the trend results shown earlier in Figure 3,  
307 superimposing upon those our estimates of the trends that would result if  $K_{zz}$  in WACCM  
308 increased at 25%, 33% and 50% per decade. Above about 10<sup>-2</sup> hPa, where CO<sub>2</sub> is no longer  
309 well mixed, changes in  $K_{zz}$  begin to impact the CO<sub>x</sub> trend, and a trend of 33% per decade in  
310  $K_{zz}$  gives the best match to the observed trend in CO<sub>x</sub> below about 2 x 10<sup>-4</sup> hPa (95 km).  
311 Above that altitude there are substantial differences between the estimated WACCM trend  
312 and the ACE-FTS trend; better agreement might have been achieved by limiting the altitude  
313 range over which  $K_{zz}$  changes, but we have avoided any such arbitrary modifications, if for  
314 no other reason that they would have required additional calculations that are not easily  
315 implemented in the model. A similar mismatch between the modeled and observed trend  
316 profiles occurred when *Emmert et al.* used a one-dimensional model to support their  
317 argument for an increase in the rate of vertical diffusion (cf. their Figure 2). Thus, neither  
318 the results presented in Figure 7 nor those of *Emmert et al.* produce a completely

319 satisfactory agreement between modeled and observed trends of  $\text{CO}_x$ , although they are  
320 able to match the observed trends over much of the lower thermosphere.

321 Similar results are obtained when trends in  $\text{CO}_2$  alone are considered, as shown in  
322 Figure 8. Again, a decadal increase in  $K_{zz}$  of about a third would bring the WACCM trend  
323 of  $\text{CO}_2$  into line with the trend obtained from ACE-FTS data. Incidentally, the ACE-FTS  
324 trend of CO is statistically indistinguishable from zero everywhere above 90 km (not  
325 shown). Thus, the discrepancy in modeled versus observed trends in  $\text{CO}_x$  is dominated by  
326 the behavior of  $\text{CO}_2$ , at least below 100-105 km, where most of the total carbon resides in  
327  $\text{CO}_2$ . The very large trend in  $\text{CO}_2$  obtained from ACE-FTS data (which exceeds 12% near  
328 105 km) is consistent with the recent study of *Yue et al.* [2015], who estimated the trend in  
329  $\text{CO}_2$  from observations made by the SABER instrument onboard NASA's TIMED satellite  
330 from 2002 through 2014. *Yue et al.* reported a trend of  $\sim 10\%$  per decade above 105 km; as  
331 shown in their Figure 2, the trend profile derived from SABER differs from the ACE-FTS  
332 trend profile in that the trend peaks at a higher altitude, but is consistent with ACE-FTS  
333 insofar as the trend in the lower thermosphere is much larger than the trend below 80 km.

334 Taken together, the SABER and ACE-FTS results make a strong case for a fast  
335 increase in  $\text{CO}_2$  in the lower thermosphere in recent years. WACCM simulations, on the  
336 other hand, produce trends that are everywhere indistinguishable from the trend at lower  
337 altitudes, which can be ascribed to anthropogenic emissions of  $\text{CO}_2$ . Estimates of the  
338 impact of  $K_{zz}$  on modeled trends suggest that an increase in eddy vertical mixing can bring  
339 the model results into agreement with observations. This is consistent with the conclusions  
340 of *Emmert et al.* [2012], who obtained a similar result using the one-dimensional, diffusive  
341 model of *Roble* [1995]. The required change in  $K_{zz}$  ranges from 15% per decade in the

342 calculations of *Emmert et al.* to over 30% per decade in the estimates presented here. The  
343 parameterization of gravity wave breaking included in WACCM is designed to interact  
344 with the resolved dynamics of the underlying model, as discussed in Section 2, but fails to  
345 produce a significant change in  $K_{zz}$  in the MLT over the period considered here (or indeed,  
346 over any period in the late 20<sup>th</sup> and early 21<sup>st</sup> centuries; not shown). Furthermore, there is  
347 essentially no direct evidence for a recent global increase in turbulent mixing, although the  
348 work of *Hoffman et al.* [2011] suggests a local increase in gravity wave activity over  
349 Juliusruh, Germany (55°N).

350 In view of the foregoing results, one might wonder whether it is possible to find  
351 additional, independent evidence for a rapid increase in eddy vertical mixing in the MLT  
352 since the early 2000s. Insofar as there are no global, long-term observations of gravity  
353 wave breaking in the MLT, evidence for a global increase in  $K_{zz}$  would have to come from  
354 global observations of minor species that are expected to respond sensitively to vertical  
355 mixing. We have examined the impact of  $K_{zz}$  in WACCM on several species, including  
356 atomic oxygen (which can be estimated from ozone and OH airglow observed by SABER,  
357 and is measured by the SCIAMACHY instrument on the Envisat satellite [*Zhu et al.*,  
358 2015]), and water vapor (which has been measured by SABER but not yet released as a  
359 validated data product). As regards atomic oxygen, Smith et al. (2009) have shown that its  
360 vertical profile is affected by vertical diffusion. However, wWe find that, even though O  
361 exhibits a very steep vertical gradient above 80 km, it is not very sensitive to changes in  $K_{zz}$   
362 in WACCM. This happens because the vertical gradient of O is shallow at the altitudes  
363 where its photochemical lifetime is long, and steep mainly where it photochemical lifetime  
364 is short, which reduces the impact of transport on the local mixing ratio. Even a 50%

365 change in  $K_{zz}$  produces changes in WACCM O whose magnitude is less than 10% (not  
366 shown).

367 Water vapor, on the other hand, may be a potentially useful indicator of changes in  $K_{zz}$ .  
368 Water vapor is photolyzed by Lyman-alpha radiation above about 80 km, but the rate of  
369 photolysis is slow enough (days to weeks) that the vertical gradient is strongly influenced  
370 by eddy mixing. Figure 9 shows the estimated impact of trends in  $K_{zz}$  on the trend of water  
371 vapor. Between about 85 and 95 km ( $3 \times 10^{-3}$  to  $5 \times 10^{-4}$  hPa), where the H<sub>2</sub>O mixing ratio  
372 in WACCM varies from about 1 ppmv to 0.5 ppmv (not shown), a 33% per decade trend in  
373  $K_{zz}$  would produce a trend in H<sub>2</sub>O varying from 15% per decade at 85 km to 30% per  
374 decade at 95 km. This is substantially larger than the trend below the mesopause (~7% per  
375 decade), which in WACCM arises mainly from specified anthropogenic emissions of  
376 methane and a slight warming of the cold point tropopause during the period of interest.  
377 Above 95 km, the trend in H<sub>2</sub>O produced by increasing  $K_{zz}$  is even larger than at lower  
378 altitudes, but the local mixing ratio is much less than 1 ppmv, likely making it impossible to  
379 retrieve its abundance accurately.

380 *Nedoluha et al.* [2009] studied the evolution of water vapor in the mesosphere, up to  
381 about 80 km, during solar cycle 23. They compared observations made by the Water Vapor  
382 Millimeter-wave Spectrometer (WVMS) with data from HALOE (Halogen Occultation  
383 Experiment) and other instruments that together covered the period 1992-2008. After  
384 accounting for the impact of changes in Lyman-alpha radiation over the solar cycle,  
385 *Nedoluha et al.* found that HALOE water vapor increased by about 8-9% between 60 and  
386 80 km from 1992 through 1996; on the other hand, from 1996 through 2005 (the last year  
387 of HALOE observations), water vapor decreased slightly in both HALOE and WVMS. To

388 put these findings in perspective, the WACCM water vapor trend over the decade 1992-  
389 2001 (which encompasses the period of increase documented by *Nedoluha et al.*), is  $\sim 8 \pm$   
390 7% at 80 km and  $\sim 13 \pm 12\%$  at 90 km (not shown); this may be compared to the nearly  
391 altitude independent  $7 \pm 10\%$  per decade obtained for 2004-2013 (Figure 9). The trend in  
392  $K_{zz}$  calculated by WACCM over the period 1992-2001 is also statistically indistinguishable  
393 from zero (not shown). Evidently, WACCM water vapor can exhibit substantial inter-  
394 decadal variability, comparable to that seen in the observations analyzed by *Nedoluha et*  
395 *al.*, that is unrelated to eddy transport and could complicate the attribution of decadal  
396 trends. Nevertheless, the estimated impact of changes in  $K_{zz}$  illustrated in Figure 9 is large  
397 enough (15-30% per decade at 85-95 km) that it ought to be discernible even in the  
398 presence of variability arising from other sources.

399 In summary, the evidence from the observations considered in this study points to a  
400 fast rate of increase in  $\text{CO}_2$  in the lower thermosphere that cannot be simulated with our  
401 state of the art climate-chemistry model. In order for WACCM to produce trends of  $\text{CO}_x$   
402 and  $\text{CO}_2$  in the lower thermosphere consistent with ACE-FTS and SABER observations,  
403 vertical eddy diffusion would have to increase substantially (at an estimated rate of over  
404 30% per decade). Examination of suitable datasets for other minor species (e.g., water  
405 vapor) in the lower thermosphere would be desirable to provide independent confirmation  
406 of such a rapid rate of increase in turbulent mixing.

407  
408 **Acknowledgments.** The Atmospheric Chemistry Experiment (ACE), also known as  
409 SCISAT, is a Canadian-led mission supported mainly by the Canadian Space Agency and  
410 the Natural Sciences and Engineering Research Council of Canada; we thank Kaley Walker  
411 for helping us access the ACE data and advising us on its use. We are also indebted to

412 Anne K. Smith and William Randel for their comments and suggestions on the original  
413 version of this work; and to Marty Mlynczak and two anonymous reviewers for additional  
414 comments, all of which have resulted in an improved paper. The National Center for  
415 Atmospheric Research (NCAR) is sponsored by the U.S. National Science Foundation. R.  
416 R. Garcia and D. R. Marsh were supported in part by NASA grants X09AJ83G and  
417 NNX13AE33G, respectively. M. López-Puertas and B. Funke were supported by  
418 MINECO (Spain) under grant ESP2014-54362-P, and EC FEDER funds. WACCM is a  
419 component of NCAR’s Community Earth System Model (CESM), which is supported by  
420 the National Science Foundation (NSF) and the Office of Science of the U.S. Department  
421 of Energy. Computing resources were provided by NCAR’s Climate Simulation  
422 Laboratory, sponsored by NSF and other agencies. This research was enabled by the  
423 computational and storage resources of NCAR’s Computational and Information Systems  
424 Laboratory (CISL). The model output and data used in this paper is listed in the references  
425 or available from the authors.

- 427 Ball, W. T., N. A. Krivova, Y. C. Unruh, J. D. Haigh and S. K. Solanki (2014), A new  
428 SATIRE-S Spectral Solar Irradiance reconstruction for solar cycles 21–23 and its  
429 implications for stratospheric ozone, *J. Atmos. Sci.*, **71**, 4086–4101, 2014.
- 430 Beagley, S. R., C. D. Boone, V. I. Fomichev, J. J. Jin, K. Semeniuk, J. C. McConnell, and  
431 P. F. Bernath (2010), First multi-year occultation observations of CO<sub>2</sub> in the MLT by  
432 ACE satellite: Observations and analysis using the extended CMAM, *Atmos. Chem.*  
433 *Phys.*, **9**, 1133–1153.
- 434 Boone, C. D., R. Nassar, K. A. Walker, Y. Rochon (2005), Retrievals for the atmospheric  
435 chemistry experiment Fourier-transform spectrometer, *Appl. Opt.*, **44** (33), 7218–7231.
- 436 Boone, C. D., Walker, K. A., and Bernath, P. F. (2013), Version 3 Retrievals for the  
437 Atmospheric Chemistry Experiment Fourier Transform Spectrometer (ACE-FTS). In  
438 *The Atmospheric Chemistry Experiment ACE at 10: A Solar Occultation Anthology*, A.  
439 Deepak Publishing, Hampton, Virginia, USA, 103–127.
- 440 Clerbaux, C. et al. (2008), CO measurements from the ACE-FTS satellite instrument: data  
441 analysis and validation using ground-based, airborne and spaceborne observations,  
442 *Atmos. Chem. Phys.*, **8**, 2569–2594.
- 443 Emmert, J. T., M.H. Stephens, P. F. Bernath, D. P. Drob and C. D. Boone (2012),  
444 Observations of increasing carbon dioxide concentrations in the Earth’s thermosphere,  
445 *Nature Geoscience*, **5**, 868–871, doi:10.1038/ngeo1626.
- 446 Ermolli, I., et al., Recent variability of the solar spectral irradiance and its impact on  
447 climate modeling, *Atmos. Chem. Phys.*, **13**, 3945–3977, 2013.

448 Fischer, H., et al. (2008), MIPAS: An instrument for atmospheric and climate research,  
449 *Atmos. Chem. Phys.*, **8**, 2151–2188.

450 Funke, B. et al. (2009), Carbon monoxide distributions from the upper troposphere to the  
451 mesosphere inferred from 4.7 $\mu$ m non-local thermal equilibrium emissions measured by  
452 MIPAS on ENVISAT, *Atmos. Chem. Phys.*, **9** (7), 2387–2411.

453 Garcia, R. R., D. R. Marsh, D. E. Kinnison, B. A. Boville, and F. Sassi (2007), Simulation  
454 of secular trends in the middle atmosphere, 1950-2003, *J. Geophys. Res.*, **112**, D09301,  
455 doi:10.1029/2006JD007485.

456 Garcia, R. R., M. López-Puertas, B. Funke, D. R. Marsh, D. E. Kinnison, A. K. Smith, and  
457 F. González-Galindo (2014), On the distribution of CO<sub>2</sub> and CO in the mesosphere and  
458 lower thermosphere, *J. Geophys. Res.*, **119**, 5700-5718, doi:10.1002/2013JD021208.

459 Hoffmann, P., M. Rapp, W. Singer, and D. Keuer (2011), Trends of mesospheric gravity  
460 waves at northern middle latitudes during summer, *J. Geophys. Res.*, **116**, D00P08,  
461 doi:10.1029/2011JD015717.

462 Krivova, N., S. K. Solanki, and Y. C. Unruh (2011), Towards a long-term record of solar  
463 total and spectral irradiance. *J. Atmos. Sol.-Terr. Phys.*, **73**, 223–234,  
464 doi:10.1016/j.jastp.2009.11. 013.

465 Kunz, A., L. L. Pan, P. Konopka, D. E. Kinnison, and S. Tilmes (2011), Chemical and  
466 dynamical discontinuity at the extratropical tropopause based on START08 and  
467 WACCM analysis, *J. Geophys. Res.*, **116**, D24302, doi:10.1029/2011JD016686.

468 Lean, J. L., G. J. Rottman, H. L. Kyle, T. N. Wood, J. R. Hickey and L. C. Puga (1997),  
469 Detection and parameterization of variations in solar mid- and near-ultraviolet radiation  
470 (200-400 nm), *J. Geophys. Res.*, **102**, 29,329-29,956.

471 Liu, H.-L., F. Sassi and R. R. Garcia (2009), Error growth in a whole atmosphere climate  
472 model, *J. Atmos. Sci.*, **66**, 173-186.

473 Nedoluha, G. E., R. M. Gomez, B. C. Hicks, J. E. Wrotny, C. Boone, and Alyn Lambert  
474 (2009), Water vapor measurements in the mesosphere from Mauna Loa over solar cycle  
475 23, *J. Geophys. Res.*, **114**, D23303, doi: 10.1029/2009JD012504.

476 Oelhaf, H., MIPAS Mission Plan (2008), ESA Technical Note ENVI- SPPA-EOPG-TN-07-  
477 0073.

478 Richter, J. H., F. Sassi, and R. R. Garcia (2010), Toward a physically based gravity wave  
479 source parameterization in a general circulation model, *J. Atmos. Sci.*, **67**, 136-156.

480 Rienecker, M. M., et al. (2011), MERRA: NASA's Modern-Era Retrospective Analysis for  
481 Research and Applications, *Journal of Climate*, **24**, 3624-3648, doi:10.1175/JCLI-D-  
482 11-00015.1.

483 Roble, R. G. (1995), Energetics of the mesosphere and thermosphere, in The Upper  
484 Mesosphere and Lower Thermosphere: A Review of Experiment and Theory, *Geophys.*  
485 *Monogr. Ser.*, vol. **87**, edited by R. M. Johnson and T. L. Killeen, pp. 1-21, AGU,  
486 Washington, D. C., doi:10.1029/GM087p0001.

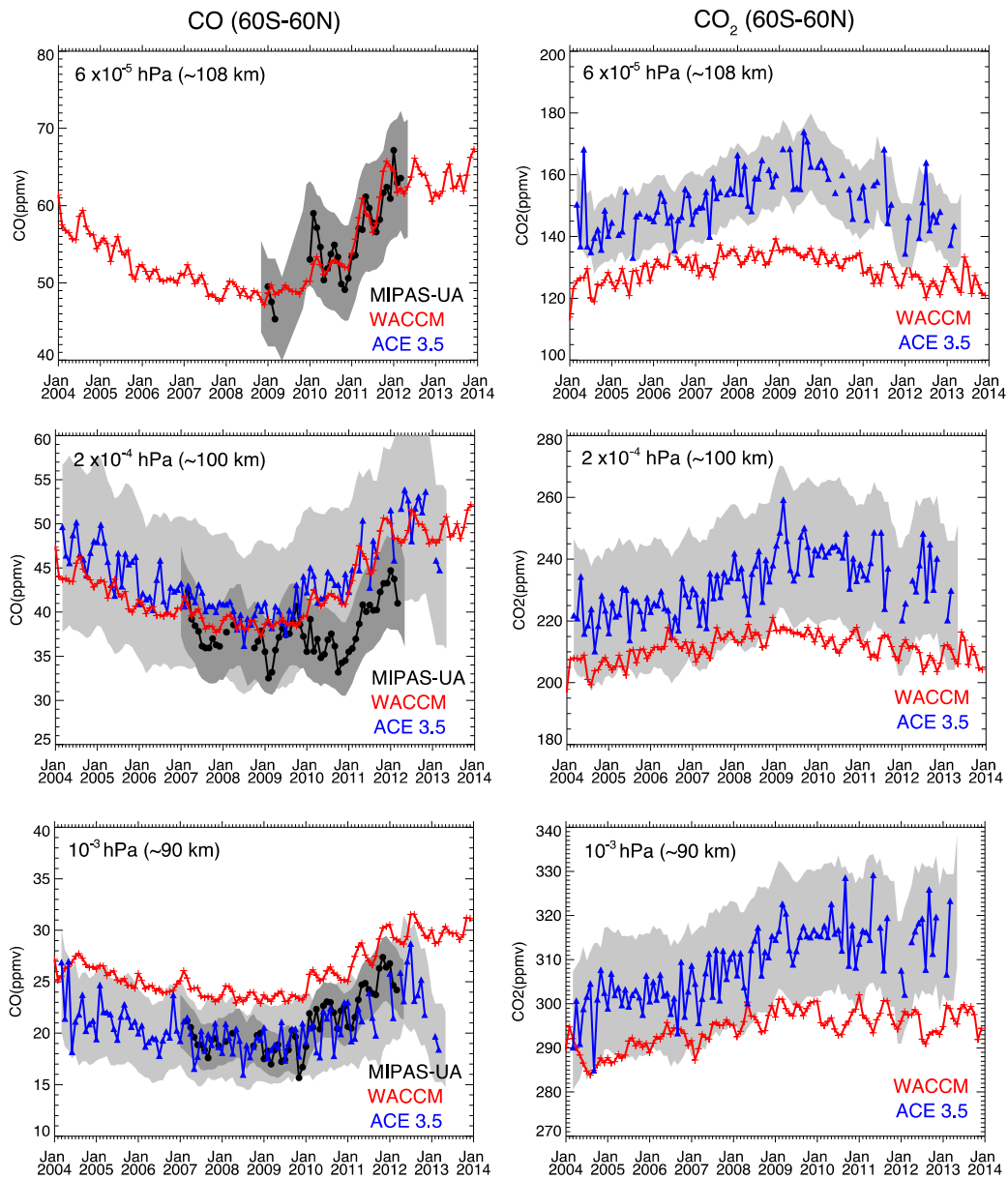
487 Smith, A. K., D. R. Marsh, M. G. Mlynczak, and J. C. Mast (2010): Temporal variations of  
488 atomic oxygen in the upper mesosphere from SABER, *J. Geophys. Res.*, **115**, D18309,  
489 doi:10.1029/2009JD013434.

490 Tiao, G. C., G. C. Reinsel, D. Xu, J. H. Pedrick, X. Zhu, A. J. Miller, J. J. DeLuisi, C. L.  
491 Mateer, and D. J. Wuebbles (1990), Effects of autocorrelation and temporal sampling  
492 schemes on estimates of trend and spatial correlation, *J. Geophys. Res.*, **95**, 20,507-  
493 20,517.

494 Yue, J., J. Russell III, Y. Jian, L. Rezac, R. Garcia, M. López-Puertas, and M. G. Mlynczak  
495 (2015), Increasing carbon dioxide concentration in the upper atmosphere observed by  
496 SABER, *Geophys. Res. Lett.*, **42**, doi:10.1002/2015GL064696.

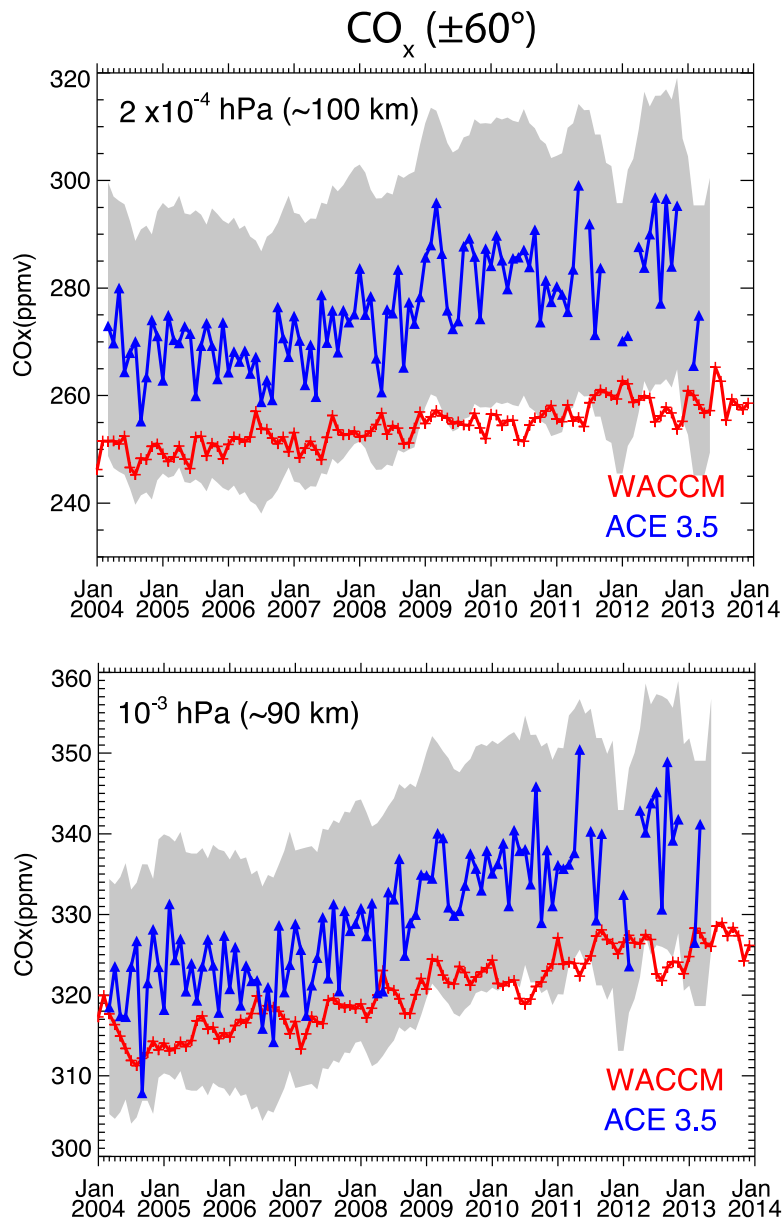
497 Zhu, Y., M. Kaufmann, M. Ern, and M. Riese: Nighttime atomic oxygen in the mesopause  
498 region retrieved from SCIAMACHY O(<sup>1</sup>S) green line measurements and its response to  
499 solar cycle variations (2015), *J. Geophys. Res.*, doi: 10.1002/2015JA021405.

500



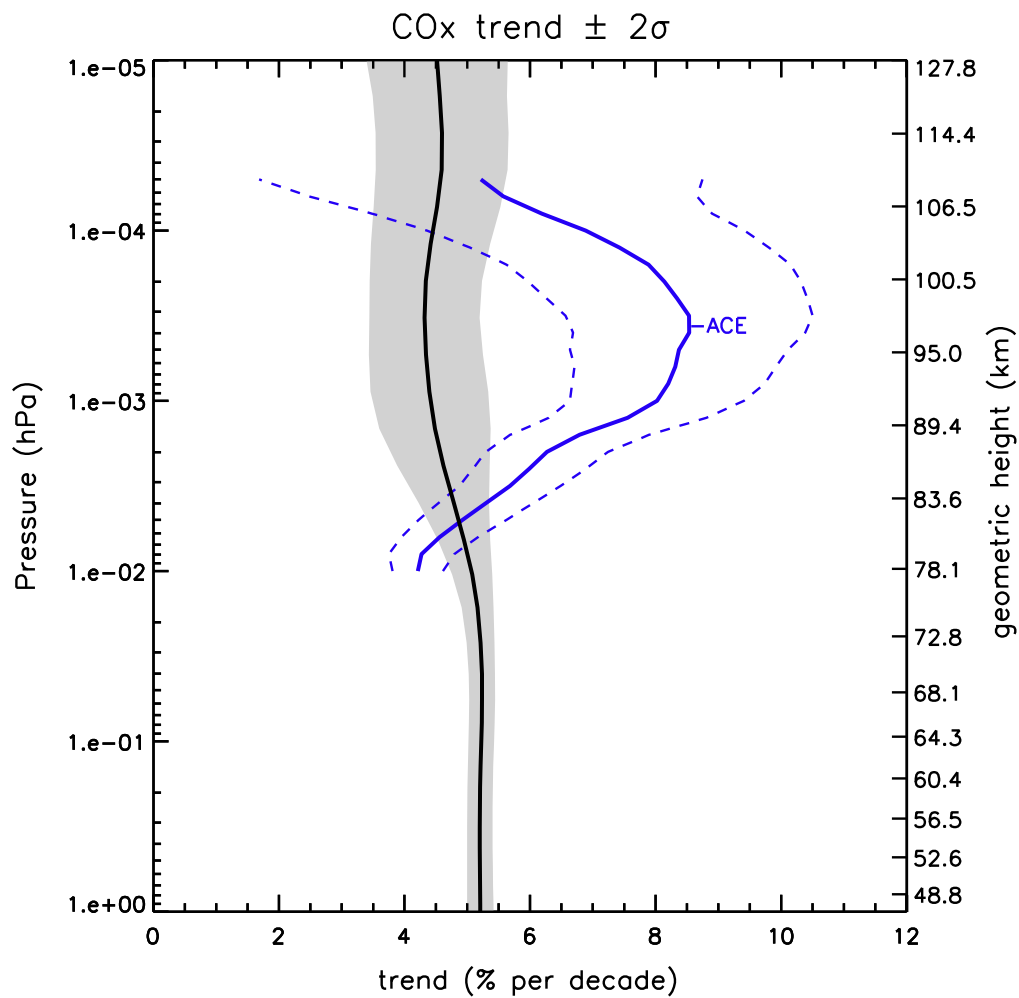
501

502 Figure 1. Evolution of observed and modeled CO (left) and CO<sub>2</sub> (right) averaged over 60S-  
 503 60N for 2004-2013 at three pressure levels. Black and blue curves denote MIPAS and ACE  
 504 data, respectively, with systematic measurement errors shaded; WACCM results are shown  
 505 in red.



506

507 Figure 2. Evolution of observed and modeled  $\text{CO}_x$  averaged over 60S-60N for the period  
 508 2004-2013 at  $2 \times 10^{-4} \text{ hPa}$  and  $10^{-3} \text{ hPa}$ . Blue curves denote ACE data, with systematic  
 509 errors shaded; WACCM results are shown in red.

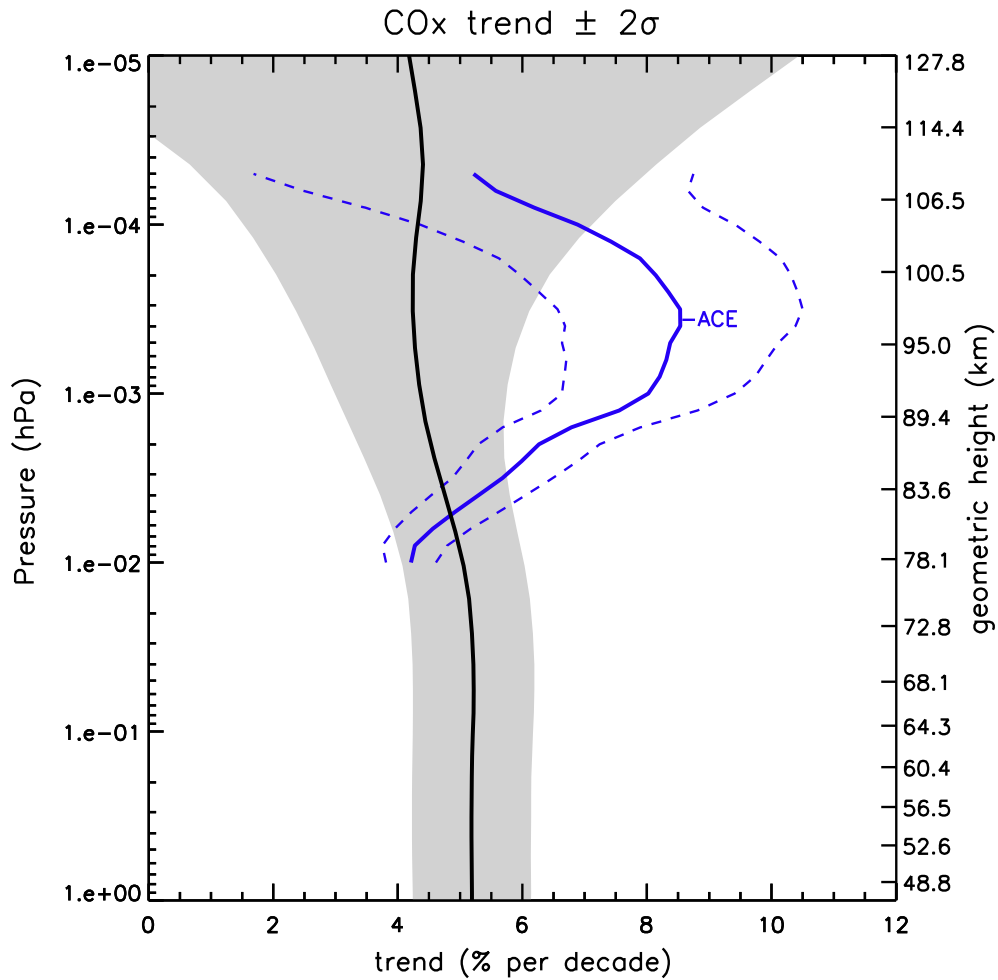


510

511 Figure 3. Vertical profile of the global trend (% per decade) of CO<sub>x</sub> = CO + CO<sub>2</sub> for the  
 512 period 2004-2013 derived from ACE observations (blue) and WACCM results (black).

513 Dashed lines and gray shading denote 2-sigma uncertainties of the ACE and WACCM

514 trend estimates, respectively.



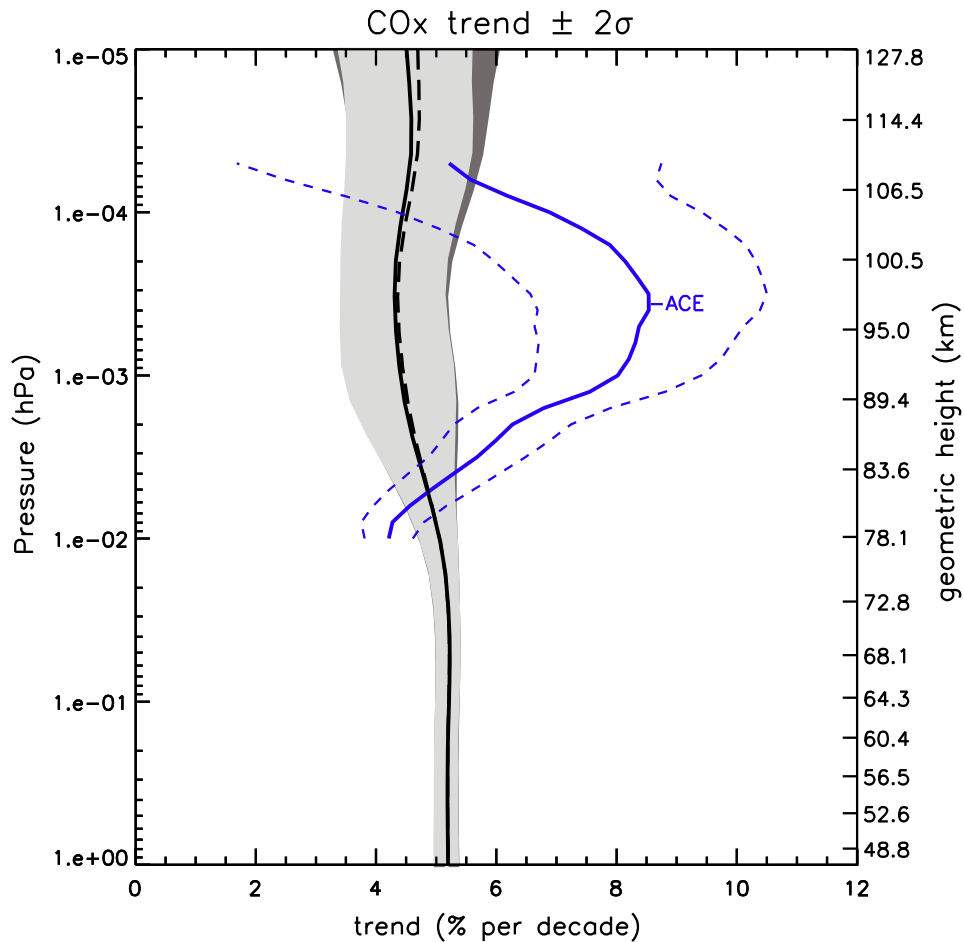
515

516 Figure 4. Effect on the WACCM CO<sub>x</sub> trend of adding random noise to the model output.

517 The blue curve denotes the trend derived from ACE; dashed lines and gray shading denote

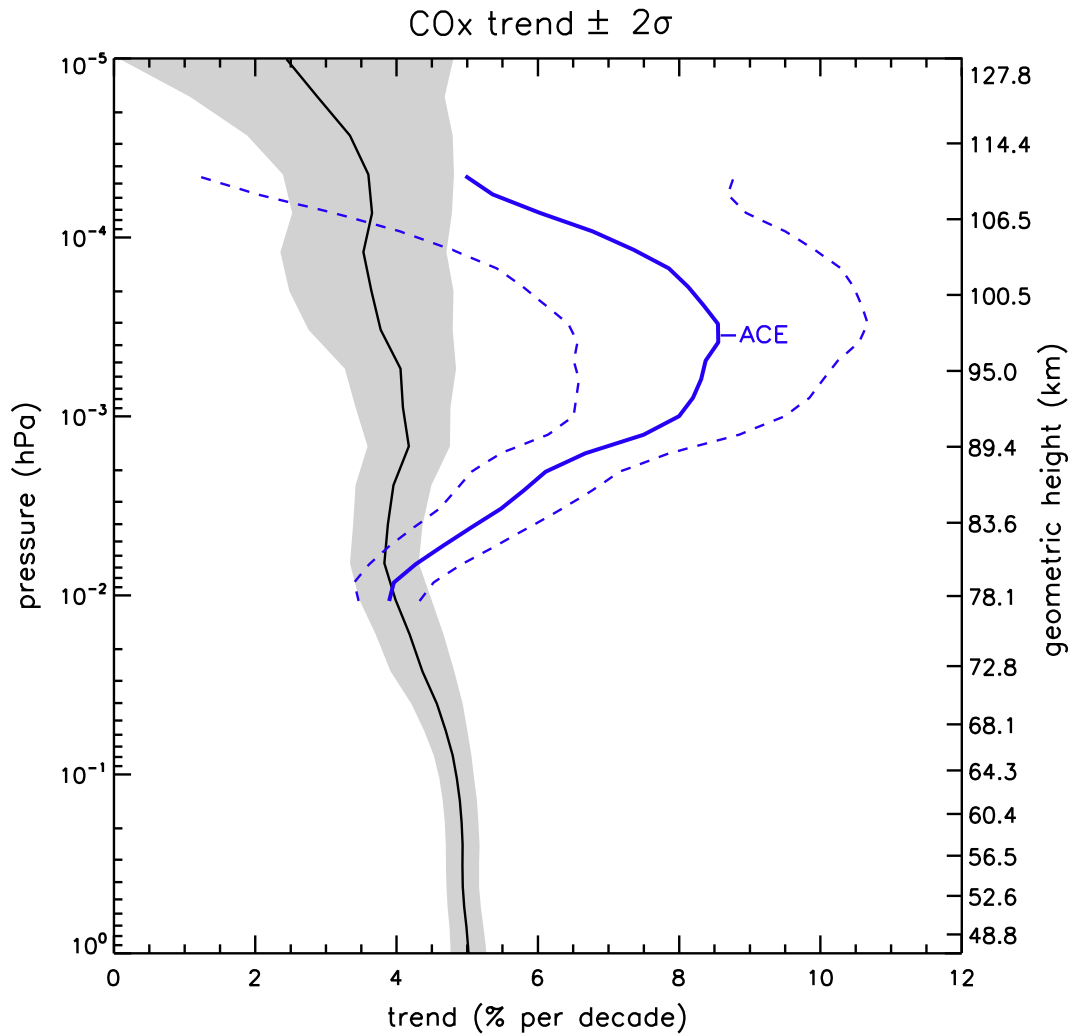
518 2-sigma uncertainties of the ACE and WACCM trend estimates, respectively. See text for

519 details.



520

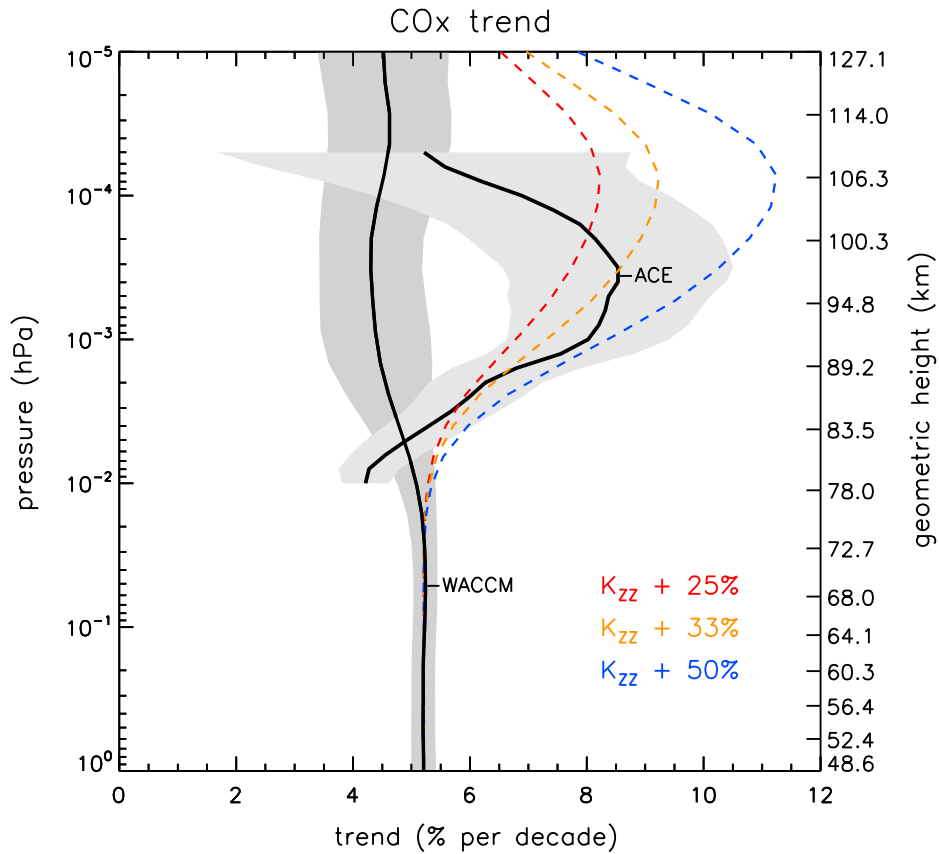
521 Figure 5. Effect on the WACCM CO<sub>x</sub> trend of doubling the solar cycle irradiance variation  
 522 at 120-200 nm. The solid curve and light shading denote the trend from the original  
 523 simulation and its uncertainty; the dashed curved and dark shading refer to the simulation  
 524 with increased irradiance variability. The blue curve and dashed lines denote the ACE trend  
 525 and its uncertainty. See text for details.



526

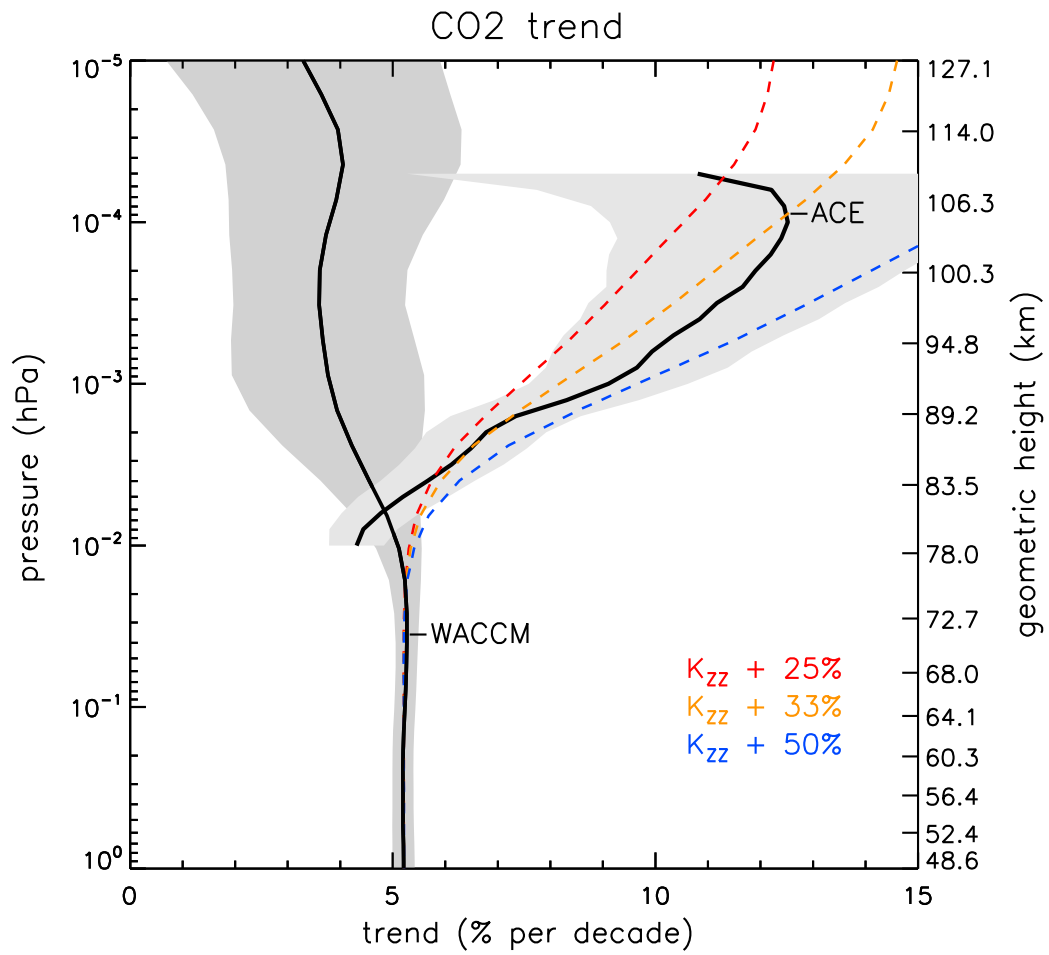
527 Figure 6. The WACCM CO<sub>x</sub> trend obtained when the model is sampled at the geo-locations  
 528 of the ACE-FTS observations compared with the trend obtained from ACE data;  
 529 uncertainties are denoted by shading and dashed lines, respectively. See text for details.

530



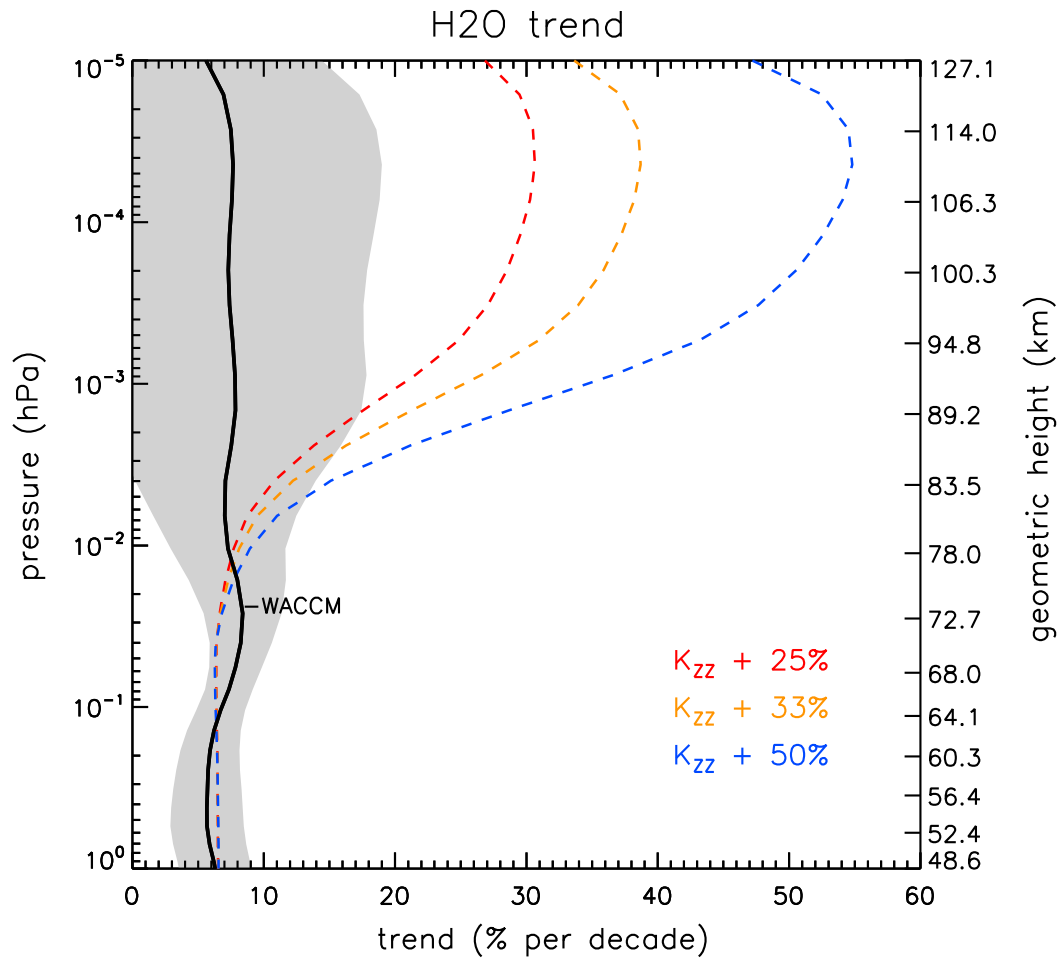
531

532 Figure 7. Effect of changing  $K_{zz}$  on the WACCM trend of  $\text{CO}_x$ . ACE and WACCM trends  
 533 for 2004-2013 are denoted by the black curves, with gray shading indicating 2-sigma  
 534 uncertainties. The estimated impact on WACCM results of increasing  $K_{zz}$  by 25%, 33% and  
 535 50% per decade is illustrated by the colored dashed curves. See text for details.



536

537 Figure 8. As in Figure 7, but for the trend of CO<sub>2</sub>.



538

539 Figure 9. As in Figure 7, but for the trend of H<sub>2</sub>O.